ACS APPLIED MATERIALS & INTERFACES

Research Article

www.acsami.org

Layered Protonated Titanate Nanosheets Synthesized with a Simple One-Step, Low-Temperature, Urea-Modulated Method as an Effective Pollutant Adsorbent

Cheng-Hsien Lin, David Shan-Hill Wong,* and Shih-Yuan Lu*

Department of Chemical Engineering, National Tsing Hua University, Hsinchu 30013, Taiwan

ABSTRACT: A simple one-step, low-temperature, urea-modulated method is developed for the synthesis of layered protonated titanate nanosheets (LPTNs). Urea serves as an indirect ammonium ion source, and the controlled supply of the ammonium ion slows the crystalline formation process and enables the production of the LPTNs from amorphous intermediate through aging-induced restructuring. The resulting LPTNs exhibit excellent adsorption capacities for methylene blue and Pb^{2+} because of their high specific surface areas and excellent ion-exchange capability. Intercalation of Pb^{2+} into the interlayer space of the LPTNs is evidenced by the relevant X-ray diffraction patterns on perturbation of the layered structure. The LPTNs prove to be a promising adsorbent in wastewater treatment for adsorption removal of metal ions or cationic organic dyes.

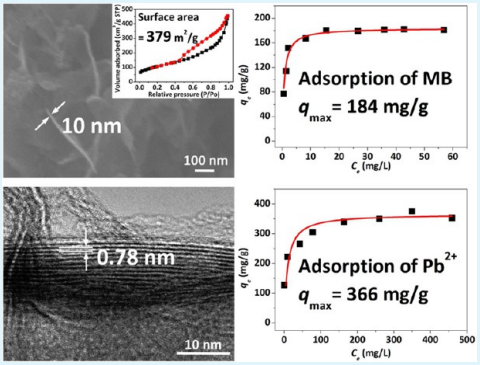

KEYWORDS: *layered materials, protonated titanate, nanosheet, adsorbent, methylene blue, lead*

INTRODUCTION

Since Kasuga et al.[1] first reported a simple hydrothermal synthesis for the preparation of TiO_2 nanotubes, layered protonated titanates (LPTs), including nanotubes, nanofibers, and nanosheets, have received tremendous research attention because of their excellent physiochemical properties and wide range of applications, such as in solar cells, catalysts, lithium ion batteries, adsorbents, and so on.[2,3] Recently, titanate nanotubes were deposited into large tintanium oxide nanotubes to create a hierarchical tube-in-tube structure, which can significantly increase the adsorption capacity of dye.[4] The crystallographic structure of LPTs has been well-investigated, and the titanate layers consist of TiO_6 octahedral units connected through edge- and corner-sharing, with small positive ions residing in the interlayers counterbalancing the negative charges of the titanate layers.[2,3] Conventional methods to synthesize layered titanates can be divided into two main categories, namely, alkali wet methods and solid-state methods. The alkali wet method synthesizes layered titanates by dissolving titanium precursors (anatase or rutile) in a concentrated alkali solution (NaOH[5−9] or KOH[7−9]) at elevated temperatures (above or equal 100 °C), and the mixture goes through a hydrothermal[5,7,9] or refluxing[6,8] treatment. On the other hand, the solid-state method produces layered titanates by calcining the mixture of TiO_2 powders and alkali carbonates (Cs_2CO_3,[10,11] Na_2CO_3,[12,13] or K_2CO_3[14]) at high temperatures, usually ranging from 600 to 1000 °C. The products of the above two methods are metal titanates. A subsequent ion-exchange procedure to exchange metal ions with protons, provided by HCl or HNO_3, is necessary to obtain the final LPTs. Compared with the solid-state method, the alkali wet method is more popular because of its less severe thermal conditions. However, in the alkali wet method, owing to the asymmetrical chemical environment[15] or mechanical tension[16] developed during the reaction, the obtained titanates usually exhibit elongated morphologies (like nanotubes or nanofibers), consisting of folded layers of nanosheets.[5−9] "Unfolded" titanate nanosheets may also be obtained hydrothermally by adjusting experimental conditions such as temperature, reaction time, and concentration of the alkali solution. A subsequent additional ion-exchange procedure is, however, still required to prepare LPTs.[17−21]

In recent years, direct synthesis approaches of layered protonated titanate nanosheets (LPTNs), without the additional ion-exchange procedure, have been developed. Takezawa and Imai[22,23] reported the synthesis of LPTNs by using agar gels containing TiF_4 in NH_4OH solution as a matrix to control the diffusion of the ionic species and to provide a mild reaction environment to form LPTNs. Jitputti et al.[24] reported a hydrothermal synthesis of flowerlike LPTNs by first synthesizing spherical amorphous titania followed by a hydrothermal treatment in an NH_4OH solution. Chen et al.[25] produced spiky LPTN beads through hydrothermal treatment of previously prepared amorphous precursor beads in an NH_4OH solution. Although the above-mentioned hydrothermal methods did not require an ion-exchange procedure, they need to first obtain the amorphous precursors. Consequently, these methods are considered two-step processes. Zhao et al.[26] fabricated LPTNs with a one-step approach in which titanium *n*-butoxide

Received: June 4, 2014
Accepted: September 8, 2014
Published: September 8, 2014

   dx.doi.org/10.1021/am5035335 | *ACS Appl. Mater. Interfaces* 2014, 6, 16669−16678

(TBOT) directly reacted with the NH_4OH solution hydrothermally. They also tested the influence of NaCl concentration in the NH_4OH solution on the resultant products at different temperatures.[27] Their results showed that well-defined LPTNs were obtained at temperatures above 100 °C. Gao et al.[28] also developed a one-pot synthesis method of LPTNs by taking TBOT as the precursor in an NH_4OH solution for hydrothermal treatments. Very recently, the use of TBOT as the precursor to react with nitrogen-containing solvents such as hexamethylenetetramine,[29] *N*,*N*-dimethylformamide,[30] and monohydrate hydrazine[31] generated LPTNs under hydrothermal conditions. Many of the above hydrothermal methods required the use of aqueous ammonia solutions. This requires the use of an autoclave in laboratory because of the high pressure involved. Leakage will result in the release of highly concentrated ammonia. These are important hazardous concerns if the process is scaled up for industrial production. A room-temperature process was developed by Sutradhar et al.[32] in which LPTNs were prepared from a peroxo-titanium carbonate precursor. The synthesized materials were granular in nature, although nanosheets were also observed. The specific surface area of the product was 96 m^2/g, and the maximum adsorption capacity of Pb^{2+} was 206 mg/g. Only with a hydrothermal treatment at 110 °C for 24 h, a hierarchical structure, in which LPTNs were assembled into hollow spheres of a high specific surface area of 334 m^2/g and Pb^{2+} removal capacity of 333 mg/g, was achieved.[33]

To summarize, most one-step processes produce LPTNs under hydrothermal conditions at temperatures greater than 100 °C. Hence a pressurized vessel is required. A chemical reagent capable of providing NH_4^+ ions or other ammino-derivatives is also required.[22−33] A low-temperature (100 °C), atmospheric pressure method without using autoclave to fabricate titanates ($H_2Ti_3O_7$) was proposed by Bavykin et al.[8] In this work, the obtained titanates were nanotubular metal titanates, and a subsequent ion-exchange procedure was essential to obtain prontonated layered titinate structure. In this work, we report a simple one-step synthesis of LPTNs with the assistance of urea, reacting in ambient atmosphere at low temperatures (90 °C) without using an autoclave and a subsequent ion-exchange procedure. The function of urea is for controlled generation of NH_4^+ ions, which can be intercalated into the interlayer space of the TiO_6 layers. At a temperature greater than 80 °C, the hydrolysis of the urea solution[34] provides NH_4^+ ions and a suitable basic condition (pH ≈ 9) to form LPTNs.[23,35]

$$(NH_2)_2CO + 3H_2O \rightarrow 2NH_4^+ + 2OH^- + CO_2 \qquad (1)$$

The effects of the reaction time and concentration of the urea solution are investigated in this study, and the results indicate that both factors play an important role in LPTN formation. The resultant LPTNs possess porous structure and have large surface area up to 379 m^2/g. Adsorption experiments reveal that the as-prepared LPTNs possess high adsorption capacities of model pollutants MB and Pb^{2+} ions, showing that LPTNs are promising pollutant adsorbents in wastewater treatment.

EXPERIMENTAL SECTION

Chemicals. Titanium *n*-butoxide (TBOT, 99+ %), serving as the source of titanium, is purchased from Alfa Aesar. Urea (99%), absolute ethanol (≥99.8%), methylene blue (MB, ≥82%), nitric acid (70%), and ammonium hydroxide (28%) are purchased from Sigma-Aldrich. All chemical reagents described in this article are used as received without further purification, and deionized water (DI-water, Milli-Q, 18.2 MΩ cm) is used in all relevant experiments.

Synthesis of LPTNs. In a typical run, 3.2 mol of urea is dissolved in 200 mL of deionized (DI) water in a single-necked flask under vigorous stirring. The flask is then sealed with a Teflon-twined glass stopper and preheated to 90 °C in an oil bath. After approximately 1 h, when the temperature of the content reaches steady state, 0.008 mol of TBOT is added into the flask. The mixture is then aged at 90 °C for 7d. The resulting white powders are collected by centrifugation, washed with ethanol, and finally dried at 60 °C overnight.

To investigate the influence of the urea concentration and aging time, a series of experiments with different molar ratios of urea to TBOT (400, 200, 100, 50, 25, 10, and 0) and aging times (1 and 7 d) was conducted. The resulting samples were denoted with sample- as the prefix followed by the molar ratio of urea to TBOT (x) and the aging time (y d) in the general form of "sample-x-y". For instance, a sample name of sample-400−7 stands for samples obtained with the molar ratio of urea to TBOT being 400 and aging time being 7 d. The DI water volume of 200 mL and process temperature of 90 °C were used in all LPTN synthesis experiments.

Characterizations. The morphologies and structures of the samples were characterized by a field emission scanning electron microscope (FESEM, JEOL, JSM-7000F, 10 kV) and a high-resolution transmission electron microscope (HRTEM, JEOL, ARM200F, 200 kV). Powder X-ray diffraction (XRD) measurements were conducted using a powder diffractometer (Rigaku, Ultima IV) with Cu Kα radiation (λ = 1.5406 Å) operating at a scan rate of 2°/min over the 2θ range of 5 to 70°. Chemical compositions of the samples were analyzed with an X-ray photoelectron spectroscope (XPS, PHI, Quantera SXM). Nitrogen adsorption/desorption isotherms were recorded at 77 K using an ASAP2020 instrument from Micromeritics. The samples are degassed at 100 °C for 8 h under vacuum before the analysis. The specific surface areas of the samples are determined with the Brunauer−Emmett−Teller (BET) model using the adsorption isotherm in the relative pressure (P/P_0) range of 0.06 to 0.3. The pore-size distributions of the samples are calculated with the Barrett−Joyner−Halenda (BJH) model based on the desorption isotherm. The zeta potential is measured with a Malvern Nano ZS.

Adsorption Experiments. For adsorption experiments, two model pollutants, namely, cationic organic dye MB and heavy metal Pb^{2+}, were used to test the adsorption abilities of LPTNs. All the adsorption experiments were conducted at room temperature under constant stirring. For adsorption of MB, the pH values of the MB solutions were adjusted to 9.5−10 by ammonium hydroxide before the adsorption experiment. To determine the adsorption kinetics and equilibrium time of adsorption, three experiments were carried out. In each run, 10 mg of LPTNs was added to 40 mL of MB solutions of initial concentrations of 30, 50, and 100 mg/L. At progressing times, aliquots were withdrawn from the solutions and diluted with a proper volume of DI water prior to quantitative analyses of the MB concentration. The MB concentrations were determined by measuring the absorption intensity at the characteristic wavelength of 664 nm using a UV−visible spectrophotometer (Hitachi, U-2800). The intensities were converted to concentrations using a standard calibration curve. The sampling continued until the MB concentration became constant, that is, the adsorption process reaches its equilibrium. For adsorption of Pb^{2+}, the pH values of the aqueous solutions of $Pb(NO_3)_2$ are first adjusted to about 5 by HNO_3. LPTNs (10 mg) were added to 25 mL of $Pb(NO_3)_2$ solutions of initial concentrations of 50 and 150 mg/L. Aliquots at different times were withdrawn and filtered, and Pb^{2+} concentrations were estimated by inductively coupled plasma atomic emission spectroscopy (ICP-AES, Agilent 725) until the concentration reached its equilibrium. The amount of adsorbate absorbed q_t (mg/g) at time t (min) and adsorption capacity q_e (mg/g) at equilibrium were determined as follows:

$$q_t = \frac{(C_0 - C_t)V}{W} \qquad (2)$$

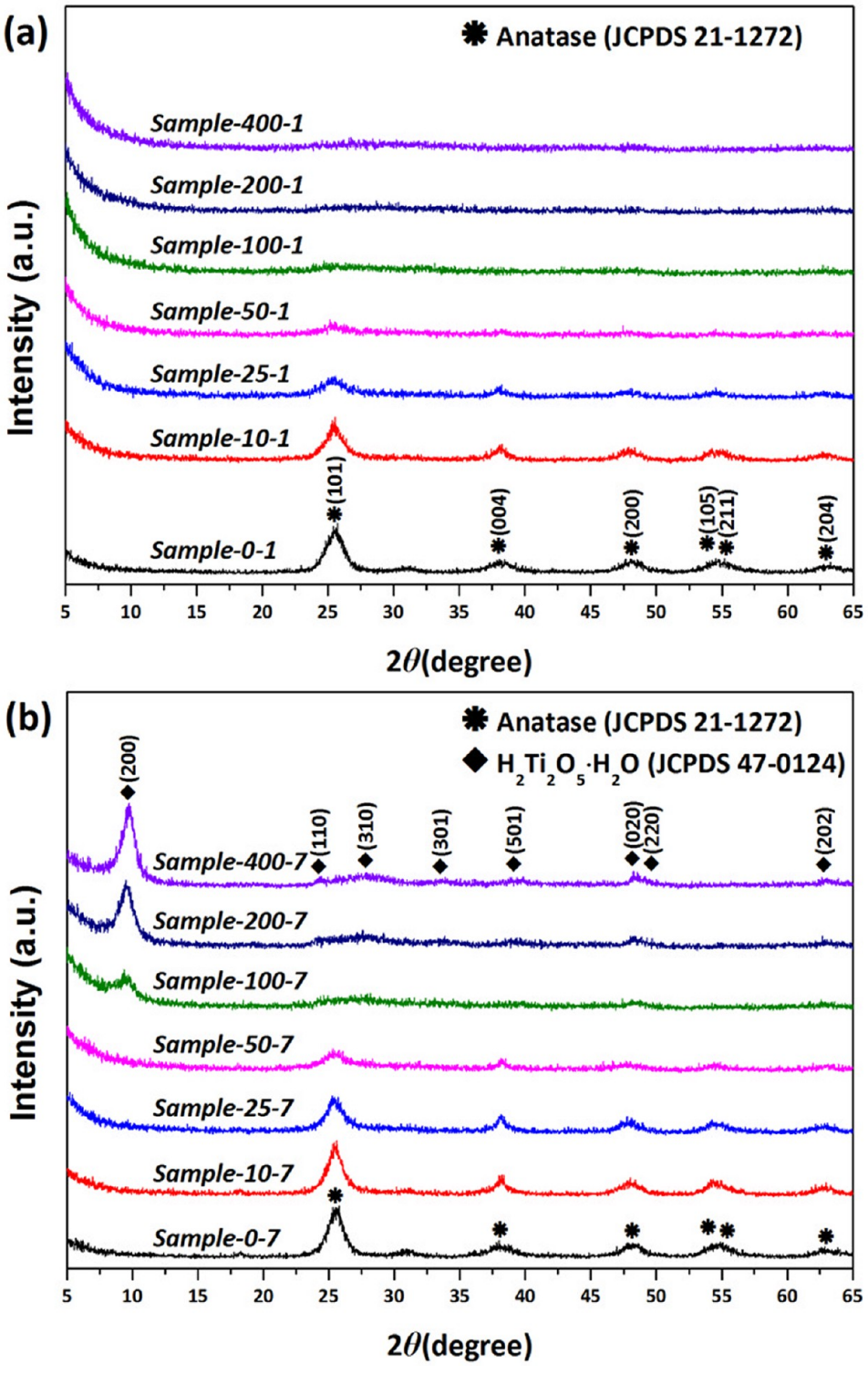

Figure 1. Powder XRD patterns of as-synthesized LPTNs with different molar ratios of urea to TBOT and aging times of (a) 1 d and (b) 7 d.

$$q_e = \frac{(C_0 - C_e)V}{W} \quad (3)$$

where C_0 (mg/L), C_t (mg/L), and C_e (mg/L) are concentrations of the adsorbate at initial, time t, and equilibrium, respectively. V (mL) is the volume of pollutant solution, and W (g) is the total addition amount of the LPTNs. To determine the equilibrium adsorption isotherm and maximum adsorption capacity of adsorbate absorbed onto the LPTNs, experiments with different initial concentrations of MB and $Pb(NO_3)_2$ solutions are conducted. The adsorption capacities of MB and Pb^{2+} are calculated based on data collected from the adsorption experiments with initial concentrations ranging from 20 to 100 mg/L and 50 to 600 mg/L, respectively.

RESULTS AND DISCUSSION

Powder XRD, SEM, and TEM. The crystalline structure of the as-synthesized samples is studied with powder XRD as shown in Figure 1. For the case of 1 d aging, the product of the control case, obtained without the addition of urea, shows

Scheme 1. A Proposed Formation Mechanism for the Layered Titanate and Anatase TiO_2

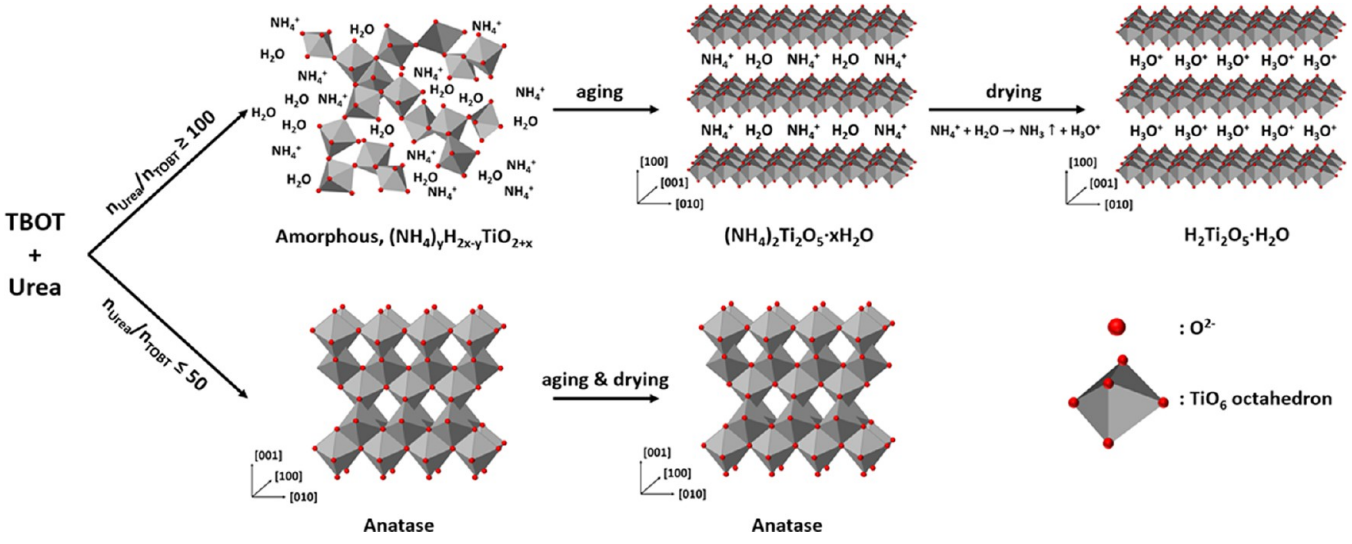

pronounced diffraction patterns of anatase. Diffraction peaks at 2θ values of 25.4, 37.8, 48.1, 53.9, 55.1, and 62.7° can be indexed to the (101), (004), (200), (105), (211), and (204) lattice planes of anatase TiO_2 (JCPDS 21−1272) (Figure 1a). Once urea is introduced to the synthetic system, the crystallinity of the product turns weak and almost disappears with the molar ratio of urea to TBOT increasing to 50. When the molar ratio of urea to TBOT reaches 100 or higher, no identifiable diffraction peaks can be observed, indicating amorphous products. The above-observed trend implies that the introduction of urea retards the crystalline formation of the product.

With the aging time increasing to 7 d, it is observed that the initial anatase structure, identified for products synthesized with the molar ratio of urea to TBOT of 50 or less, is retained and better developed. This is expected. Interestingly, for samples that are initially under the 1 d aging condition, a strong diffraction peak at $2\theta \approx 9.7°$ emerges when the aging time is prolonged to 7 d. This low angle diffraction peak is characteristic of layered crystalline structure. As the molar ratio of urea to TBOT increases, the intensity of the low-angle characteristic peak also increases. Sample-400−7 exhibits the most well-developed crystalline structure among the three layered products, as judged from the relatively more well-defined diffraction pattern. Diffraction peaks at 2θ of 9.7, 24.1, 27.8, 33.4, 39.1, 48.1, and 62.9° correspond well to the (200), (110), (310), (301), (501), (020), and (002) lattice planes of layered protonated titanate $H_2Ti_2O_5{\cdot}H_2O$ (JCPDS 47−0124), respectively (Figure 1b).

As shown in Scheme 1, a mechanism is proposed to explain the observed trend. First, the precursor, TBOT, a titanium alkoxide, reacts with water to produce titanium oxides.[36] If there are no NH_4^+ ions present in the solution, anatase TiO_2 is obtained because of the rearrangement of the condensing TiO_6 octahedral monomers. When there are NH_4^+ ions present in the solution ($n_{urea}/n_{TBOT} \leq 50$), the rearrangement of the TiO_6 octahedral monomers to produce anatase TiO_2 is interrupted, resulting in a decrease in product crystallinity. Here, n_{urea} and n_{TBOT} are mole numbers of urea and TBOT, respectively. When there are sufficient NH_4^+ ions present in the solution ($n_{urea}/n_{TBOT} \geq 100$), the TiO_6 octahedral monomers are separated by the intercalation of NH_4^+ ions, which results in the formation of the amorphous titanate of $(NH_4)_yH_{2x-y}TiO_{2+x}$.[26,27,32] During prolonged aging, the NH_4^+ ions stabilize the TiO_6 octahedral monomers to form layered structure of $(NH_4)_2Ti_2O_5{\cdot}xH_2O$.[26,27,32] Upon drying, the NH_4^+ ions intercalated in the interlayer space release NH_3 to afford the layered protonated titanate $H_2Ti_2O_5{\cdot}H_2O$ nanosheets.

Figure 2 shows the FESEM images of the anatase samples obtained with the molar ratio of urea to TBOT of less than or equal to 50. They appear as aggregates of nanoparticles, and the morphology remains almost unchanged when lengthening the aging time from 1 to 7 d, as judged from the comparison of the corresponding FESEM of Figure 2. The transformation of the amorphous samples into LPTNs is shown in Figure 3. Figure 3a−c shows that the amorphous samples, formed with 1 d of aging and molar ratio of urea to TBOT above or equal to 100, consists of both nanoparticle aggregates of major amount and nanosheets of minor amount. Figure 3d−f shows that the amorphous samples are transformed into layered $H_2Ti_2O_5{\cdot}H_2O$ nanosheets with 7 d of aging. This aging-induced crystalline structure formation is different from the processing-temperature triggered ones reported in literature for amorphous ammonium titanates $(NH_4)_2Ti_2O_5{\cdot}xH_2O$[26,27,32] and is believed to proceed through a dissolution and precipitation process.[25] Sample-400−7 exhibits the most well-developed nanosheet structure of $H_2Ti_2O_5{\cdot}H_2O$ among all samples. These FESEM images show the emergence of the nanosheet structure, in good correlation with the emergence of the characteristic low-angle diffraction peak of the layered products in the XRD patterns. Figure 3f shows that the thickness of the nanosheet is about 10 nm, corresponding to a stacking of about 11 layers of titanates according to the theoretical *d*-spacing of 0.9 nm between the (200) planes of $H_2Ti_2O_5{\cdot}H_2O$ (JCPDS 21−1272). The TEM image of sample-400−7 shown in Figure 4a reveals that the sample is composed of nanosheets of thicknesses 2−15 nm. The interlayer distance of the nanosheets as determined from the HRTEM image of Figure 4b is approximately 0.78 nm, which is smaller than the theoretical *d*-spacing of 0.9 nm of $H_2Ti_2O_5{\cdot}H_2O$. The discrepancy between the HRTEM and XRD results is usually attributed to the fact that the incidence direction of the electron beam used in the TEM imaging is not perpendicular to the layer thickness plane. A more probable reason is that the in situ dehydration, caused by the high

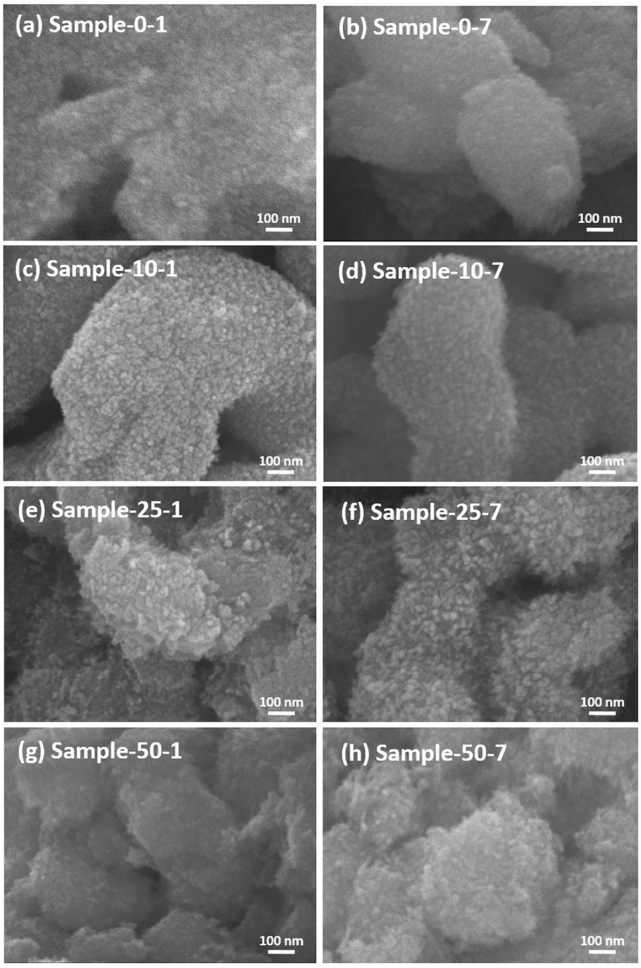

Figure 2. FESEM images of as-synthesized anatase products. (a) sample-0−1, (b) sample-0−7, (c) sample-10−1, (d) sample-10−7, (e) sample-25−1, (f) sample-25−7, (g) sample-50−1, and (h) sample-50−7.

vacuum of the TEM chamber and high energy of the electron-beam irradiation, reduces the interlayer spacing.[26,33]

BET and BJH Measurements. The specific surface areas and porosities of the as-synthesized samples are characterized using nitrogen adsorption/desorption isotherms (Table 1). It can be seen that the surface areas of the amorphous samples are much larger than those of the anatase ones for an aging time of 1 d. When the aging time is lengthened to 7 d, the surface areas of all samples of the same n_{urea}/n_{TBOT} ratio decrease. The amorphous sample is transformed into titanate structure, and its surface area decreases substantially. It is noteworthy that a large BET area of 535 m^2/g is obtained for sample-100−7. However, the crystalline structure of this sample is poor (Figure 1b). Many remnant particles can be found in the FESEM image (Figure 3d). We suspect that the large BET area of this sample may be due to incomplete transformation.

Figure 5 shows the nitrogen adsorption/desorption isotherm and corresponding BJH pore size distribution curve of sample-400−7. According to the IUPAC classification,[37] the isotherm is identified as a type IV isotherm with a type H3 hysteresis loop. A type H3 hysteresis loop is usually found on mesoporous solids consisting of aggregates of particles forming slit-shaped pores of nonuniform sizes.[38] The pore size distribution curve, inset of Figure 5, shows that the sizes of the mesopores distribute in a narrow range of 2−10 nm with the maximum pore volume occurring at the pore size of 3.72 nm. The BET surface area of sample-400−7, determined from the adsorption isotherm, reaches 379 m^2/g, which is larger than the values of typical titanate nanotubes (200−300 m^2/g)[2,3] and the values of LPTNs reported by other groups (96−350.7 m^2/g).[24,28,30,32,33] The average pore size and pore volume determined from the adsorption isotherm are 6.18 nm and 0.72 cm^3/g, respectively.

Adsorption of MB and Pb^{2+}. Layered titanates have been recognized as good adsorbents through ion exchange because of their exchangeable cations intercalated in the interlayers.[2] Their theoretical cation exchange capacity (CEC) for monovalent ions is 9.05 mmol/g,[39] much higher than the CECs of other common adsorbents, such as layered clays, zeolites, and zirconium phosphate (0.25−0.6 mmol/g).[32] In this study, we evaluate the adsorption properties of sample-400−7 using two model pollutant compounds, namely, methylene blue (MB) and lead ion (Pb^{2+}).

The evolution curves of adsorption amounts of MB and Pb^{2+} are shown in Figure 6. As can be seen in Figure 6a, the initial

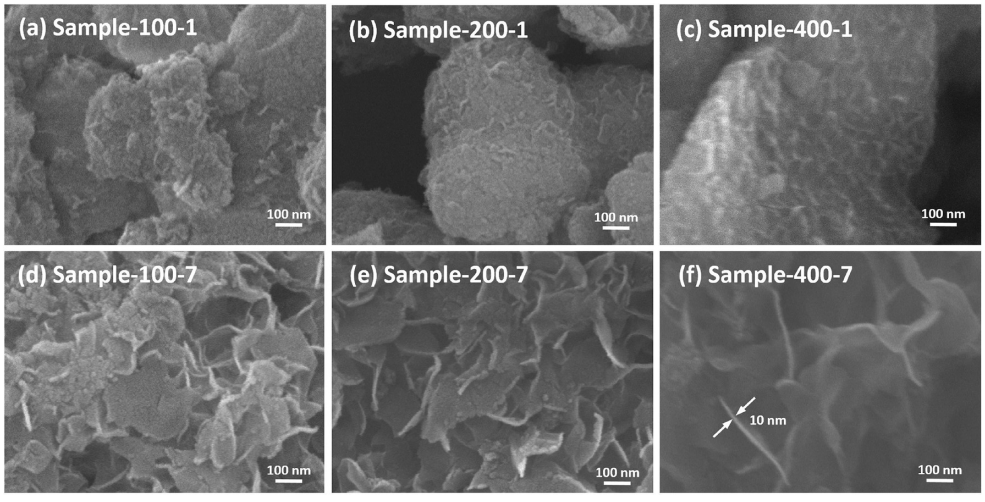

Figure 3. FESEM images of as-synthesized amorphous products, (a) sample-100−1, (b) sample-200−1 and (c) sample-400−1, and layered protonated titanate nanosheets, (d) sample-100−7, (e) sample-200−7, and (f) sample-400−7.

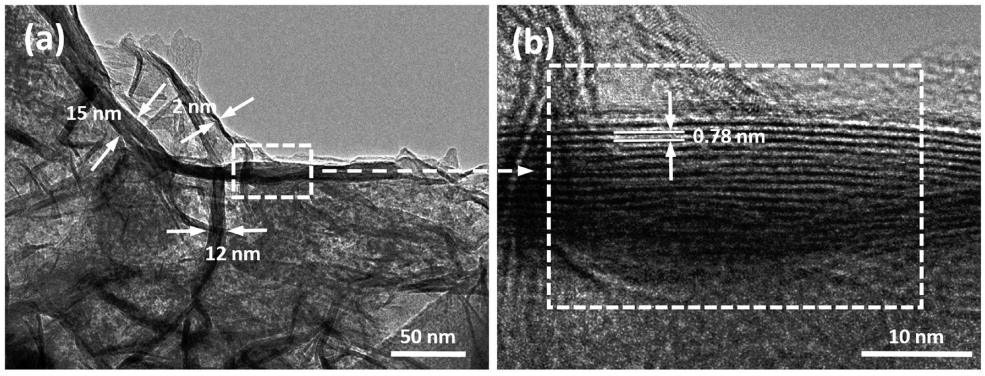

Figure 4. (a, b) HRTEM images of sample-400−7.

Table 1. Specific Surface Area, Average Pore Diameter and Average Pore Volume of Samples

sample name	S_{BET}[a] (m^2/g)	PD[b] (nm)	PV[b] (cm^3/g)	crystalline structure
sample-0−1	241	5.28	0.39	anatase
sample-10−1	385	7.31	0.56	anatase
sample-25−1	394	5.05	0.53	anatase
sample-50−1	507	4.17	0.57	anatase
sample-100−1	623	4.07	0.67	amorphous
sample-200−1	630	3.76	0.65	amorphous
sample-400−1	662	3.97	0.62	amorphous
sample-0−7	218	6.28	0.42	anatase
sample-10−7	276	8.49	0.66	anatase
sample-25−7	353	6.61	0.65	anatase
sample-50−7	469	5.44	0.7	anatase
sample-100−7	535	5.36	0.78	titanate
sample-200−7	380	6.55	0.71	titanate
sample-400−7	379	6.18	0.72	titanate

[a] S_{BET} = BET specific surface area obtained from adsorption data in the relative pressure (P/P_0) range of 0.06 to 0.3. [b] PD = average pore diameter, PV = average pore volume, determined by BJH model from the adsorption isotherm.

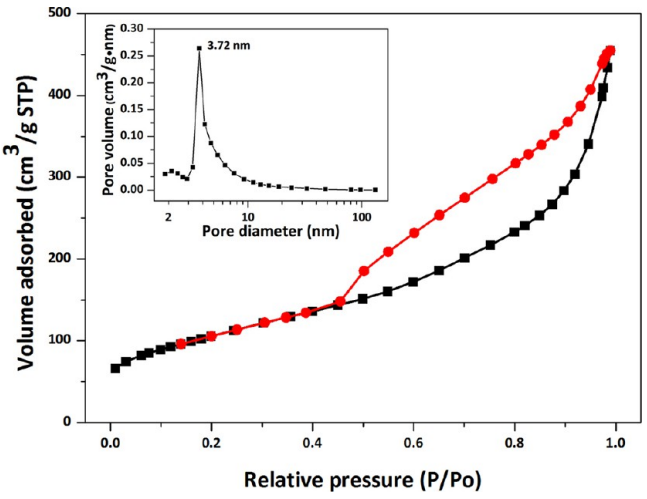

Figure 5. Nitrogen adsorption/desorption isotherm. (inset) Corresponding BJH pore size distribution curve of sample-400−7.

adsorption rate is very fast. Ninety percent of the equilibrium adsorption amount of MB is achieved within 30 min. The time needed to reach the equilibrium state varies with the corresponding initial concentration, ranging from 60 min for a low initial concentration of 30 mg/L to more than 210 min for a high initial concentration of 100 mg/L. As for Pb^{2+}, with the results shown in Figure 6b, the initial absorption is even faster, and the time needed to reach the equilibrium state is very short, approximately 10 min for a low initial concentration of 50 mg/L and 30 min for a high initial concentration of 150 mg/L. The very rapid initial adsorption may be attributed to the abundant active sites distributed on the surface of the sample.[40,41]

The adsorption evolution curves of both MB and Pb^{2+} can be fitted to the following second-order kinetic model:[42]

$$\frac{dq_e}{dt} = k(q_e - q_t)^2 \quad (4)$$

The above equation can be integrated and cast into the following form:

$$\frac{t}{q_t} = \frac{1}{kq_e^2} + \frac{1}{q_e}t \quad (5)$$

where k (g/(mg min)) is the adsorption rate constant. The values of q_e and k can be computed from the slope and intercept of the plot of t/q_t versus t. As can be seen in Figure 7, the plots of t/q_t versus t for MB and Pb^{2+} are all straight lines, implying that the adsorption processes of MB and Pb^{2+} onto the present LPTNs obey the second-order kinetic model. The fitted kinetic parameters are summarized in Table 2. The $q_{e.cal}$ values show good agreement with the experimental data, and the calculated correlation coefficients are all above 0.999, indicating excellent fit of the adsorption data with the second-order kinetic model, and the rate-controlling step is thus the chemisorption of the adsorbates.[42]

The data of adsorption amounts, q_e, and adsorbate concentrations, C_e, at equilibrium obtained at different initial adsorbate concentrations can be used to determine the adsorption isotherm model. It is found that adsorptions of both MB and Pb^{2+} can be adequately described by the Langmuir isotherm model:[43,44]

$$\frac{q_e}{q_{max}} = \frac{KC_e}{1 + KC_e} \quad (6)$$

where q_{max} (mg/g) is the monolayer maximum adsorption capacity of the adsorbate, and K (L/mg) is the Langmuir adsorption equilibrium constant. The above equation can be expressed in the following form:

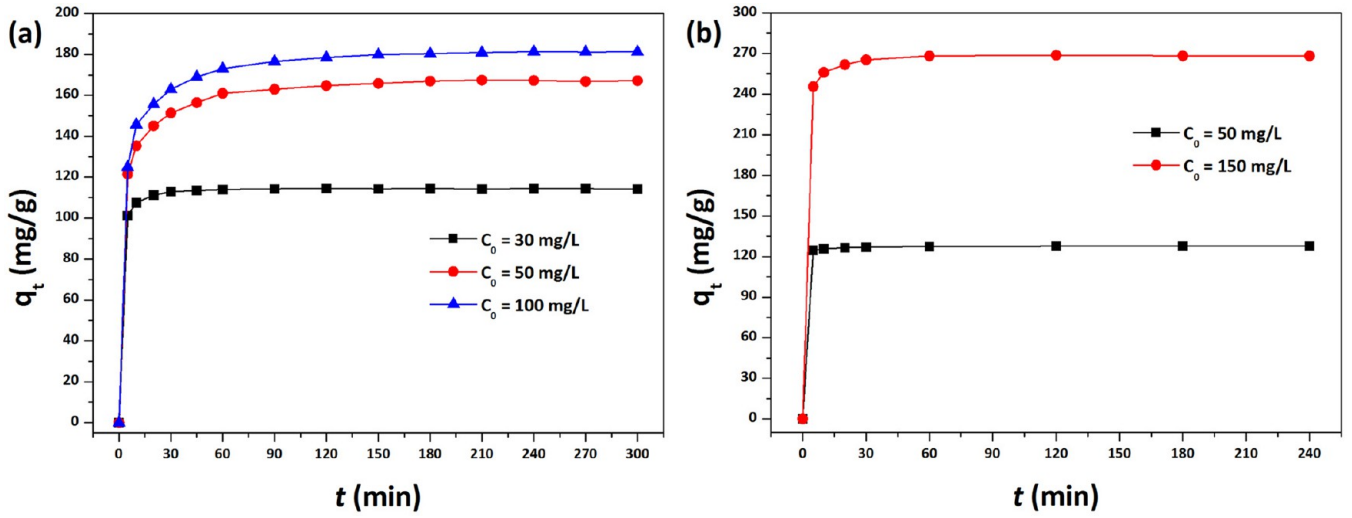

Figure 6. Effect of adsorption time on the adsorption of (a) MB and (b) Pb^{2+} onto sample-400−7 at different initial concentrations.

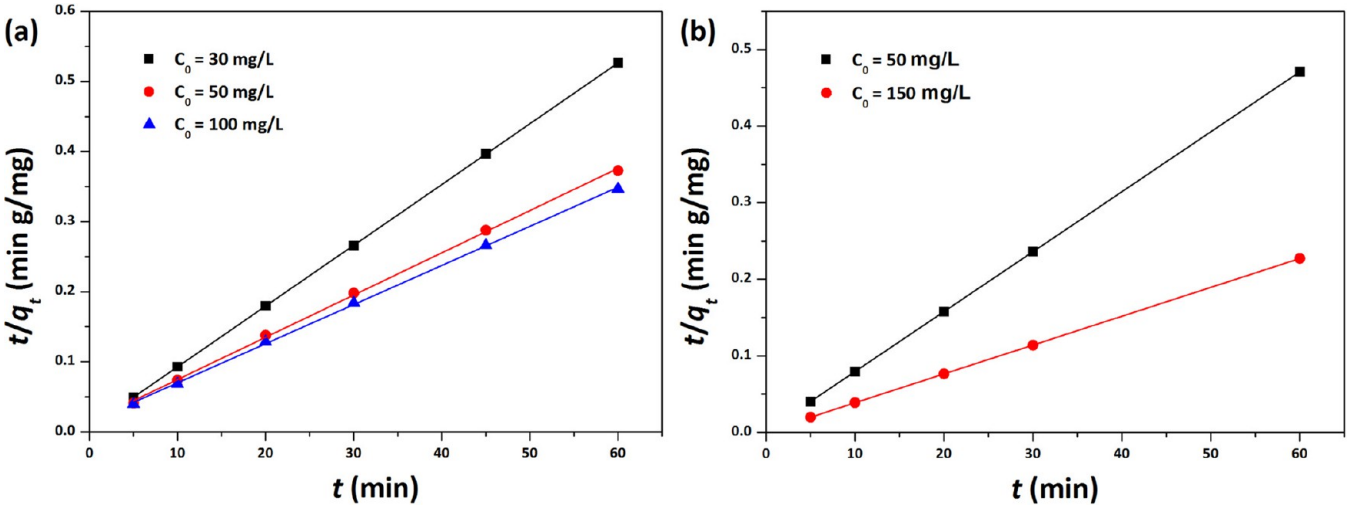

Figure 7. Second-order kinetic plot for adsorptions of (a) MB and (b) Pb^{2+} onto LPTNs-400−7.

Table 2. Second-Order Kinetic Parameters for Adsorptions of MB and Pb^{2+} onto LPTNs-400−7

	initial MB concentration (mg/L)			initial Pb^{2+} concentration (mg/L)	
parameters	30	50	100	50	150
k (g/mg min)	0.0122	0.0025	0.0022	0.0503	0.0116
$q_{e.cal}$ [a] (mg/g)	115	166	179	128	265
R^2	1.000 00	0.999 30	0.999 54	1.000 00	1.000 00
$q_{e.exp}$ [b] (mg/g)	114	167	181	128	266

[a]The calculated adsorption capacity at equilibrium according to eq 5. [b]The measured adsorption capacity at equilibrium (t = 240 min).

$$\frac{C_e}{q_e} = \frac{1}{Kq_{max}} + \frac{1}{q_{max}}C_e \quad (7)$$

The values of q_{max} and K can be computed from the slope and intercept of the plot of C_e/q_e versus C_e. The calculated parameters q_{max} and K and the indicator for goodness of fit R^2 are listed in Table 3. The high R^2 values support the fact that the Langmuir model is indeed an adequate model for the isotherms. The experimental data of adsorption capacities q_e versus equilibrium concentrations of pollutants are presented in Figure 8. It should be pointed out that the R^2 value of the Pb^{2+} isotherm is slightly inferior to the R^2 value of the MB isotherm.

Table 3. Langmuir Isotherm Constants for Adsorptions of MB and Pb^{2+} onto Sample-400−7

	pollutants	
isotherm conatants[a]	MB	Pb^{2+}
K (L/mg)	1.53	0.11
q_{max} (mg/g)	184	366
R^2	0.999 87	0.996 78

[a]Constants are calculated from eq 7.

It is caused by the deviations of experimental data at C_e = 43, 78, 350 mg/L for the Pb^{2+} adsorption data. However, there is

dx.doi.org/10.1021/am5035335 | ACS Appl. Mater. Interfaces 2014, 6, 16669−16678

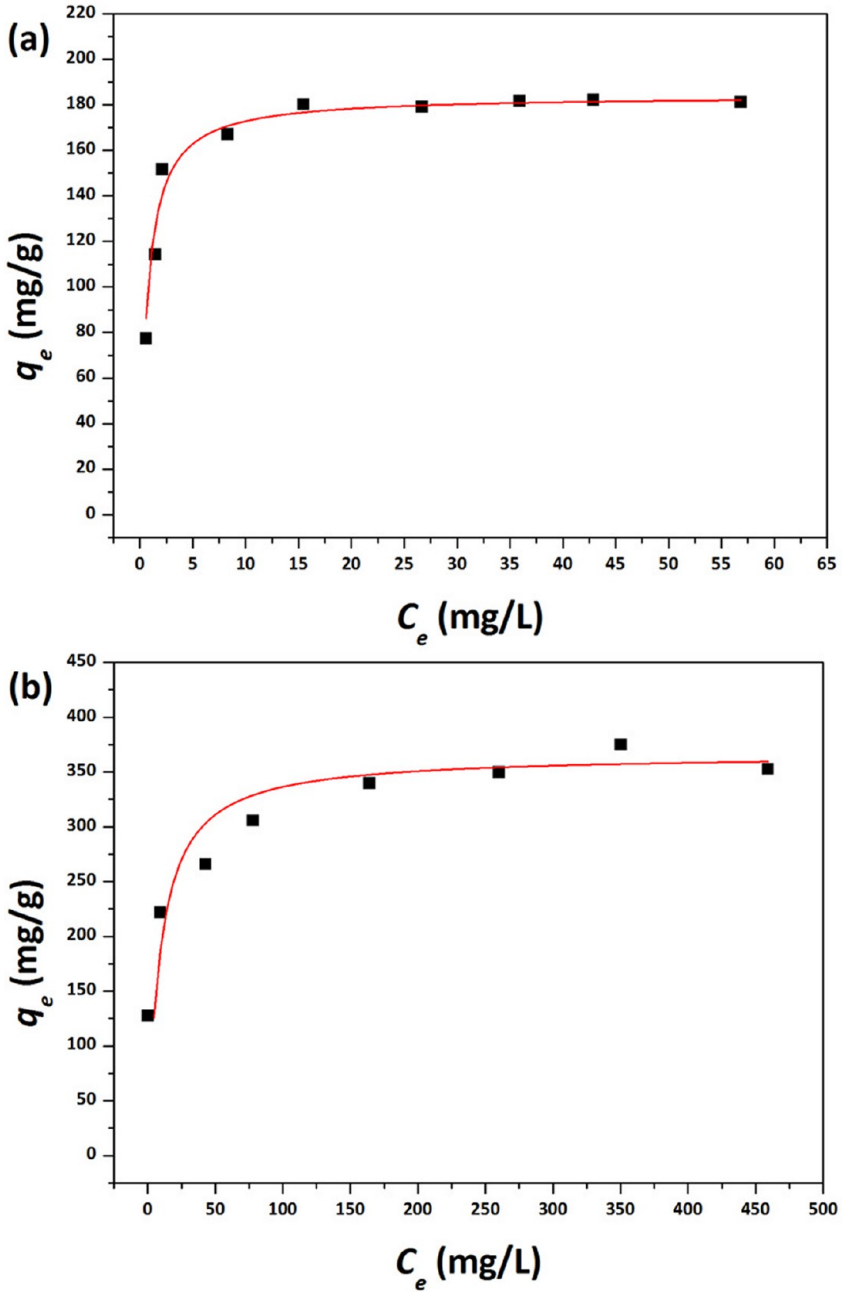

Figure 8. Langmuir isotherm plot for adsorption of (a) MB and (b) Pb^{2+} onto sample-400−7.

no statistical basis for us to reject the hypothesis that the data can be represented by a Langmuir model.

The monolayer maximum adsorption capacities are determined to be 184 and 366 mg/g for MB and Pb^{2+}, respectively (Table 3). These values compare very favorably to adsorption capacities of several common adsorbents reported in the literature, such as zeolite (16.37 mg/g, MB), activated sewage char (120 mg/g, MB), titania (6 mg/g, MB),[45] activated carbon (44 mg/g, Pb^{2+}), manganese oxide-coated zeolite (60 mg/g, Pb^{2+}), and manganese oxide-coated carbon nanotubes (79 mg/g, Pb^{2+}).[41] These values are also comparable to data reported for other layered titanate products, for example, hollow spheres (MB 154 mg/g, Pb^{2+} 323 mg/g)[33] and microspherulites (MB 236 mg/g, Pb^{2+} 499 mg/g).[39,46]

The LPTNs obtained are found to possess a negative Zeta potential of −53.6 mV in DI water. Therefore, the cationic MB molecules and Pb^{2+} can be readily adsorbed onto the surfaces of the negatively charged LPTNs because of the strong electrostatic attractions.[40,45] Whether or not the MB molecules can be intercalated into the interlayer space of the LPTNs is under dispute. Some authors suggested that MB molecules would not enter the interlayer space because MB is an organic compound of a large molecular size.[46−48] Other authors claimed that MB molecules are able to be intercalated into the interlayer space.[22,29,49] We have obtained the XRD pattern of an MB-loaded LPTN (curve (b) of Figure 9). When compared with the XRD pattern of the pristine LPTN (curve (a) of Figure 9), it is evident that the feature diffraction peak of the layered structure is not disturbed. This result suggests that MB molecules are not intercalated into the interlayer of the LPTNs.

On the other hand, it is well-known that metal ion adsorptions by layered titanates is an ion-exchange process,

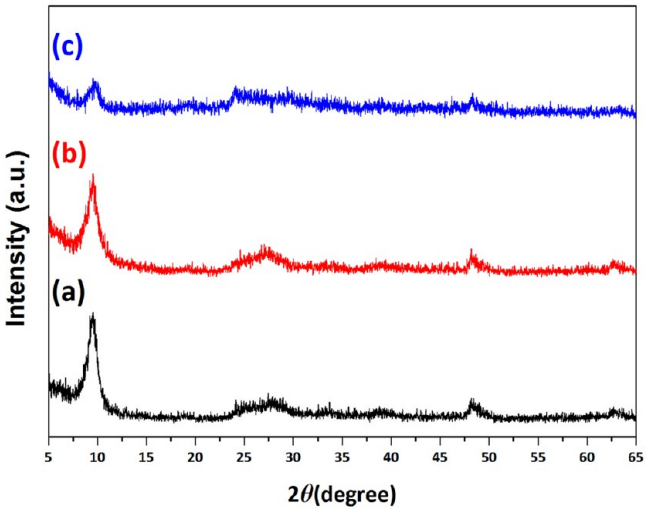

Figure 9. XRD patterns of (a) sample-400−7, (b) after adsorption of MB, and (c) after adsorption of Pb^{2+}.

which has been evidenced by relevant XRD or Raman analyses.[2,39,50] As shown as curve (c) of Figure 9, the intensity of the feature diffraction peak at about $2\theta = 9.7°$, characteristic of the layered structure, decreases dramatically when the LPTN is loaded with Pb^{2+}, implying the intercalation of Pb^{2+} into the interlayer space of the LPTNs.

CONCLUSIONS

In this study, we have successfully developed a simple one-step, low-temperature, urea-modulated synthesis of layered protonated titanate nanosheets (LPTNs), which possess high specific surface areas. The urea concentration is found to be a key factor controlling the morphology and crystalline structure of the product. With a high urea concentration, an amorphous solid is obtained that, with prolonged aging, is further transformed into layered $H_2Ti_2O_5{\cdot}H_2O$ titanates. If there is not enough urea, anatase phase product is obtained initially and would not change upon aging.

The resulting LPTNs exhibit excellent adsorption capacities for MB and Pb^{2+} because of their high specific surface areas and excellent ion-exchange capacities. Fast second-order adsorption kinetics are observed for both the MB and Pb^{2+} adsorptions, and the adsorptions can be described by the Langmuir isotherm model. The Pb^{2+} ions are intercalated into the interlayer space of the LPTN, which is supported by the relevant XRD patterns for perturbation of layered structure. The present LPTNs may be a promising adsorbent in wastewater treatments for adsorption removal of metal ions and cationic organic dyes.

The advantages of this method are that layered titanates could be directly obtained at low temperatures without an ion-exchange procedure, and a pressurized vessel is not required. The requirements of high urea concentrations in solution and a prolonged aging time are major limitations in this method. However, recycle and reuse of the urea solution is possible, and aging time can be reduced by better reactor design. Elimination of such drawbacks is an important direction for future studies.

AUTHOR INFORMATION

Corresponding Authors

*E-mail: dshwong@che.nthu.edu.tw. Phone: +886 3-5721694. (D.S.H.W.)

*E-mail: sylu@mx.nthu.edu.tw. Phone: +886 3-571436. Fax: +886 3-5715408. (S.Y.L.)

Notes

The authors declare no competing financial interest.

ACKNOWLEDGMENTS

This work was financially supported by the Ministry of Science and Technology of Taiwan under Grant Nos. NSC-101-2221-E-007-117-MY2 (D.S.H.W.) and NSC-101-2221-E-007-111-MY3 (S.Y.L.) and by the Low Carbon Energy Research Centre of the National Tsing-Hua University under Grant No. 103N2021E1.

REFERENCES

(1) Kasuga, T.; Hiramatsu, M.; Hoson, A.; Sekino, T.; Niihara, K. Formation of Titanium Oxide Nanotube. *Langmuir* **1998**, *14* (12), 3160−3163.

(2) Bavykin, D. V.; Friedrich, J. M.; Walsh, F. C. Protonated Titanates and TiO_2 Nanostructured Materials: Synthesis, Properties, and Applications. *Adv. Mater.* **2006**, *18* (21), 2807−2824.

(3) Bavykin, D. V.; Walsh, F. C. Elongated Titanate Nanostructures and Their Applications. *Eur. J. Inorg. Chem.* **2009**, *8*, 977−997.

(4) Bavykin, D. V.; Passoni, L.; Walsh, F. C. Hierarchical Tube-In-Tube Structures Prepared by Electrophoretic Deposition of Nanostructured Titanates into a TiO_2 Nanotube Array. *Chem. Commun.* **2013**, *49* (62), 7007−7009.

(5) Du, G. H.; Chen, Q.; Che, R. C.; Yuan, Z. Y.; Peng, L. M. Preparation and Structure Analysis of Titanium Oxide Nanotubes. *Appl. Phys. Lett.* **2001**, *79* (22), 3702−3704.

(6) Yang, J. J.; Jin, Z. S.; Wang, X. D.; Li, W.; Zhang, J. W.; Zhang, S. L.; Guo, X. Y.; Zhang, Z. J. Study on Composition, Structure and Formation Process of Nanotube $Na_2Ti_2O_4(OH)_2$. *Dalton Trans.* **2003**, *20*, 3898−3901.

(7) Nakahira, A.; Kato, W.; Tamai, M.; Isshiki, T.; Nishio, K.; Aritani, H. Synthesis of Nanotube from a Layered $H_2Ti_4O_9$ Center Dot H_2O in a Hydrothermal Treatment Using Various Titania Sources. *J. Mater. Sci.* **2004**, *39* (13), 4239−4245.

(8) Bavykin, D. V.; Cressey, B. A.; Light, M. E.; Walsh, F. C. An Aqueous, Alkaline Route to Titanate Nanotubes under Atmospheric Pressure Conditions. *Nanotechnology* **2008**, *19* (27), 275604.

(9) Bavykin, D. V.; Kulak, A. N.; Walsh, F. C. Metastable Nature of Titanate Nanotubes in an Alkaline Environment. *Cryst. Growth Des.* **2010**, *10* (10), 4421−4427.

(10) Sasaki, T.; Komatsu, Y.; Fujiki, Y. A New Layered Hydrous Titanium-Dioxide $H_xTi_{2-x/4}O_4{\cdot}H_2O$. *J. Chem. Soc., Chem. Commun.* **1991**, *12*, 817−818.

(11) Sasaki, T.; Watanabe, M.; Michiue, Y.; Komatsu, Y.; Izumi, F.; Takenouchi, S. Preparation and Acid-Base Properties of a Protonated Titanate with the Lepidocrocite-Like Layer Structure. *Chem. Mater.* **1995**, *7* (5), 1001−1007.

(12) Yang, J.; Li, D.; Wang, X.; Yang, X. J.; Lu, L. Study on the Synthesis and Ion-Exchange Properties of Layered Titanate $Na_2Ti_3O_7$ Powders with Different Sizes. *J. Mater. Sci.* **2003**, *38* (13), 2907−2911.

(13) Tsai, C. C.; Teng, H. Nanotube Formation from a Sodium Titanate Powder via Low-Temperature Acid Treatment. *Langmuir* **2008**, *24* (7), 3434−3438.

(14) Shen, L. M.; Bao, N. Z.; Zheng, Y. Q.; Gupta, A.; An, T. C.; Yanagisawa, K. Hydrothermal Splitting of Titanate Fibers to Single-Crystalline TiO_2 Nanostructures with Controllable Crystalline Phase, Morphology, Microstructure, and Photocatalytic Activity. *J. Phys. Chem. C* **2008**, *112* (24), 8809−8818.

(15) Zhang, S.; Peng, L. M.; Chen, Q.; Du, G. H.; Dawson, G.; Zhou, W. Z. Formation Mechanism of $H_2Ti_3O_7$ Nanotubes. *Phys. Rev. Lett.* **2003**, *91* (25), 256103.

(16) Bavykin, D. V.; Parmon, V. N.; Lapkin, A. A.; Walsh, F. C. The Effect of Hydrothermal Conditions on the Mesoporous Structure of TiO_2 Nanotubes. *J. Mater. Chem.* **2004**, *14* (22), 3370−3377.

(17) Wei, M. D.; Konishi, Y.; Arakawa, H. Synthesis and Characterization of Nanosheet-Shaped Titanium Dioxide. *J. Mater. Sci.* **2007**, *42* (2), 529−533.
(18) Peng, C. W.; Ke, T. Y.; Brohan, L.; Richard-Plouet, M.; Huang, J. C.; Puzenat, E.; Chiu, H. T.; Lee, C. Y. (101)-Exposed Anatase TiO_2 Nanosheets. *Chem. Mater.* **2008**, *20* (7), 2426−2428.
(19) Wang, C. H.; Zhang, X. T.; Zhang, Y. L.; Jia, Y.; Yang, J. K.; Sun, P. P.; Liu, Y. C. Hydrothermal Growth of Layered Titanate Nanosheet Arrays on Titanium Foil and Their Topotactic Transformation to Heterostructured TiO_2 Photocatalysts. *J. Phys. Chem. C* **2011**, *115* (45), 22276−22285.
(20) Korosi, L.; Papp, S.; Csapo, E.; Meynen, V.; Cool, P.; Dekany, I. A Short Solid-State Synthesis Leading to Titanate Compounds with Porous Structure and Nanosheet Morphology. *Microporous Mesoporous Mater.* **2012**, *147* (1), 53−58.
(21) Li, N.; Zhang, L. D.; Chen, Y. Z.; Fang, M.; Zhang, J. X.; Wang, H. M. Highly Efficient, Irreversible and Selective Ion Exchange Property of Layered Titanate Nanostructures. *Adv. Funct. Mater.* **2012**, *22* (4), 835−841.
(22) Takezawa, Y.; Imai, H. Bottom-Up Synthesis of Titanate Nanosheets with Hierarchical Structures and a High Specific Surface Area. *Small* **2006**, *2* (3), 390−393.
(23) Takezawa, Y.; Imai, H. Structural Control on Crystal Growth of Titanate in Aqueous System: Selective Production of Nanostructures of Layered Titanate and Anatase-Type Titania. *J. Cryst. Growth* **2007**, *308* (1), 117−121.
(24) Jitputti, J.; Rattanavoravipa, T.; Chuangchote, S.; Pavasupree, S.; Suzuki, Y.; Yoshikawa, S. Low Temperature Hydrothermal Synthesis of Monodispersed Flower-Like Titanate Nanosheets. *Catal. Commun.* **2009**, *10* (4), 378−382.
(25) Chen, D. H.; Huang, F. Z.; Cao, L.; Cheng, Y. B.; Caruso, R. A. Spiky Mesoporous Anatase Titania Beads: A Metastable Ammonium Titanate-Mediated Synthesis. *Chem.—Eur. J.* **2012**, *18* (43), 13762−13769.
(26) Zhao, B.; Chen, F.; Gu, X. N.; Zhang, J. L. Organic-Stabilizer-Free Synthesis of Layered Protonic Titanate Nanosheets. *Chem.—Asian J.* **2010**, *5* (7), 1546−1549.
(27) Zhao, B.; Chen, F.; Jiao, Y. C.; Zhang, J. L. Phase Transition and Morphological Evolution of Titania/Titanate Nanomaterials under Alkalescent Hydrothermal Treatment. *J. Mater. Chem.* **2010**, *20* (37), 7990−7997.
(28) Gao, Y. P.; Fang, P. F.; Liu, Z.; Chen, F. T.; Liu, Y.; Wang, D. H.; Dai, Y. Q. A Facile One-Pot Synthesis of Layered Protonated Titanate Nanosheets Loaded with Silver Nanoparticles with Enhanced Visible-Light Photocatalytic Performance. *Chem.—Asian J.* **2013**, *8* (1), 204−211.
(29) Xie, S. F.; Zheng, B. J.; Kuang, Q.; Wang, X.; Xie, Z. X.; Zheng, L. S. Synthesis of Layered Protonated Titanate Hierarchical Microspheres with Extremely Large Surface Area for Selective Adsorption of Organic Dyes. *CrystEngComm* **2012**, *14* (22), 7715−7720.
(30) Wu, H. B.; Lou, X. W.; Hng, H. H. Synthesis of Uniform Layered Protonated Titanate Hierarchical Spheres and Their Transformation to Anatase TiO_2 for Lithium-Ion Batteries. *Chem.—Eur. J.* **2012**, *18* (7), 2094−2099.
(31) Nguyen-Phan, T. D.; Oh, E. S.; Chhowalla, M.; Asefa, T.; Shin, E. W. Hierarchical Macrochanneled Layered Titanates with "House-of-Cards"-Type Titanate Nanosheets and Their Superior Photocatalytic Activity. *J. Mater. Chem. A* **2013**, *1* (26), 7690−7701.
(32) Sutradhar, N.; Sinhamahapatra, A.; Pahari, S. K.; Bajaj, H. C.; Panda, A. B. Room Temperature Synthesis of Protonated Layered Titanate Sheets Using Peroxo Titanium Carbonate Complex Solution. *Chem. Commun.* **2011**, *47* (27), 7731−7733.
(33) Sutradhar, N.; Pahari, S. K.; Jayachandran, M.; Stephan, A. M.; Nair, J. R.; Subramanian, B.; Bajaj, H. C.; Mody, H. M.; Panda, A. B. Organic Free Low Temperature Direct Synthesis of Hierarchical Protonated Layered Titanates/Anatase TiO_2 Hollow Spheres and Their Task-Specific Applications. *J. Mater. Chem. A* **2013**, *1* (32), 9122−9131.
(34) Kao, L. H.; Hsu, T. C.; Lu, H. Y. Sol-Gel Synthesis and Morphological Control of Nanocrystalline TiO_2 via Urea Treatment. *J. Colloid Interface Sci.* **2007**, *316* (1), 160−167.
(35) He, J.; Wei, M.; Li, B.; Kang, Y.; Evans, D. G.; Duan, X. Preparation of Layered Double Hydroxides. In *Layered Double Hydroxides;* Duan, X., Evans, D. G., Eds.; Springer-Verlag Berlin: Berlin, Germany, 2006; pp 89−119.
(36) Livage, J.; Henry, M.; Sanchez, C. Sol-Gel Chemistry of Transition-Metal Oxides. *Prog. Solid State Chem.* **1988**, *18* (4), 259−341.
(37) Sing, K. S. W.; Everett, D. H.; Haul, R. A. W.; Moscou, L.; Pierotti, R. A.; Rouquerol, J.; Siemieniewska, T. Reporting Physisorption Data for Gas Solid Systems with Special Reference to the Determination of Surface-Area and Porosity (Recommendations 1984). *Pure Appl. Chem.* **1985**, *57* (4), 603−619.
(38) Leofanti, G.; Padovan, M.; Tozzola, G.; Venturelli, B. Surface Area and Pore Texture of Catalysts. *Catal. Today* **1998**, *41* (1−3), 207−219.
(39) Tang, Y. X.; Lai, Y. K.; Gong, D. G.; Goh, K. H.; Lim, T. T.; Dong, Z. L.; Chen, Z. Ultrafast Synthesis of Layered Titanate Microspherulite Particles by Electrochemical Spark Discharge Spallation. *Chem.—Eur. J.* **2010**, *16* (26), 7704−7708.
(40) Rafatullah, M.; Sulaiman, O.; Hashim, R.; Ahmad, A. Adsorption of Copper (II), Chromium (III), Nickel (II) and Lead (II) Ions from Aqueous Solutions by Meranti Sawdust. *J. Hazard. Mater.* **2009**, *170* (2−3), 969−977.
(41) Xiong, L.; Chen, C.; Chen, Q.; Ni, J. R. Adsorption of Pb(II) and Cd(II) from Aqueous Solutions Using Titanate Nanotubes Prepared via Hydrothermal Method. *J. Hazard. Mater.* **2011**, *189* (3), 741−748.
(42) Ho, Y. S.; McKay, G. Sorption of Dye from Aqueous Solution by Peat. *Chem. Eng. J.* **1998**, *70* (2), 115−124.
(43) Langmuir, I. The Constitution and Fundamental Properties of Solids and Liquids. Part I. Solids. *J. Am. Chem. Soc.* **1916**, *38*, 2221−2295.
(44) Foo, K. Y.; Hameed, B. H. Insights into the Modeling of Adsorption Isotherm Systems. *Chem. Eng. J.* **2010**, *156* (1), 2−10.
(45) Xiong, L.; Yang, Y.; Mai, J. X.; Sun, W. L.; Zhang, C. Y.; Wei, D. P.; Chen, Q.; Ni, J. R. Adsorption Behavior of Methylene Blue onto Titanate Nanotubes. *Chem. Eng. J.* **2010**, *156* (2), 313−320.
(46) Tang, Y. X.; Gong, D. G.; Lai, Y. K.; Shen, Y. Q.; Zhang, Y. Y.; Huang, Y. Z.; Tao, J.; Lin, C. J.; Dong, Z. L.; Chen, Z. Hierarchical Layered Titanate Microspherulite: Formation by Electrochemical Spark Discharge Spallation and Application in Aqueous Pollutant Treatment. *J. Mater. Chem.* **2010**, *20* (45), 10169−10178.
(47) Bavykin, D. V.; Redmond, K. E.; Nias, B. P.; Kulak, A. N.; Walsh, F. C. The Effect of Ionic Charge on the Adsorption of Organic Dyes onto Titanate Nanotubes. *Aust. J. Chem.* **2010**, *63* (2), 270−275.
(48) Huang, J. Q.; Cao, Y. G.; Liu, Z. G.; Deng, Z. H.; Wang, W. C. Application of Titanate Nanoflowers for Dye Removal: A Comparative Study with Titanate Nanotubes and Nanowires. *Chem. Eng. J.* **2012**, *191*, 38−44.
(49) Feng, M.; You, W.; Wu, Z. S.; Chen, Q. D.; Zhan, H. B. Mildly Alkaline Preparation and Methylene Blue Adsorption Capacity of Hierarchical Flower-Like Sodium Titanate. *ACS Appl. Mater. Interfaces* **2013**, *5* (23), 12654−12662.
(50) Yang, D. J.; Zheng, Z. F.; Zhu, H. Y.; Liu, H. W.; Gao, X. P. Titanate Nanofibers as Intelligent Absorbents for the Removal of Radioactive Ions from Water. *Adv. Mater.* **2008**, *20* (14), 2777−2781.